

The Crustal Stress Field of Northern Chile

Carlos Herrera¹, John F. Cassidy^{2,1}, Stan E. Dosso¹, Jan Dettmer³, Wasja Bloch⁴, Christian Sippl⁵, and Pablo Salazar^{6,7}

¹School of Earth and Ocean Sciences, University of Victoria, Victoria, BC, Canada.

²Pacific Geoscience Centre, Geological Survey of Canada, Natural Resources Canada, Sidney, BC, Canada.

³Department of Geoscience, University of Calgary, Calgary, AB, Canada.

⁴Deutsches GeoForschungsZentrum, Potsdam, Germany.

⁵Institute of Geophysics, Czech Academy of Sciences, Prague, Czech Republic.

⁶Departamento de Ciencias Geológicas, Universidad Católica del Norte, Antofagasta, Chile.

⁷Centro de Investigación para la Gestión Integrada del Riesgo de Desastres (CIGIDEN), Santiago, Chile.

Corresponding author: Carlos Herrera (carlosfherrera@uvic.ca)

Key Points:

- We resolve spatial variability of the regional crustal stress field in northern Chile based on focal mechanisms of crustal earthquakes.
- Margin-parallel compressional crustal stress is observed near the coast and may be due to concave margin and friction on the interface.
- A strike-slip regime is observed towards the Andean Precordillera, where the elevated topography could affect the local stress.

Abstract

The spatial variability of the regional crustal stress in northern Chile is resolved. We infer a margin-parallel compressive crustal stress regime along the coastal region, similar to crustal stress observations in Cascadia and Japan. The Andean Precordillera shows a distinct stress field associated with a strike-slip faulting regime. These results are constrained by over a decade of observations, for which earthquake catalogs report thousands of events in the continental crust. We present focal mechanisms for 817 of these crustal earthquakes, including mechanism qualities. The best mechanisms were grouped and inverted to infer the stress-field variability. We interpret the margin-parallel compression to be caused by the concave shape of the margin and the locking of the plate interface. The inferred strike-slip regime in the Andes agrees with previous studies and has been proposed to be mostly caused by local stresses imposed by a thicker crust.

Plain Language Summary

New observations of thousands of earthquakes occurring within the continental crust (depths < 60 km) in northern Chile provide an opportunity to study the tectonic forces acting in the South American continent. We obtain fault orientations and slip directions of 817 crustal earthquakes. The orientations are used to understand the stresses that cause deformation of the crust. With hundreds of earthquakes studied, we can resolve differences in the stress between coastal and inland regions: The coastal region experiences a compression along an approximate north-south direction. Further east, near the Andes mountains, compression is nearly east-west, almost parallel to the collision direction of the tectonic plates. This could be mostly due to local stresses acting in higher topography regions. Here, earthquakes occur mostly in nearly vertical faults with slip in the horizontal direction. Conversely, the compression near the coast is likely due to the bending of this region along the coastline, in combination with the locking on the plate interface between the Nazca and South American tectonic plates. The results are remarkably similar to western North America and Japan, where the shape of plate boundaries cause similar stresses.

1 Introduction

The subduction zone in northern Chile (between 18°S and 25°S) exhibits frequent occurrence of interplate, intraslab and crustal earthquakes. Most of this seismicity is related to the relatively fast convergence rate (~63 mm/yr) of the subducting Nazca plate beneath South America in this region (Kendrick et al., 2003).

Interplate earthquakes reach the largest magnitudes, with several historical and recent large earthquakes documented (Ruiz & Madariaga, 2018). Modern seismic networks have allowed the study of the source properties and rupture mechanisms of large interplate earthquakes in northern Chile (e.g., Ruegg et al., 1996; Peyrat et al., 2010; Ruiz et al., 2014), as well as the foreshock and aftershock sequences of the 2014 Iquique earthquake (González et al., 2015; Soto et al., 2019). Source properties of large intraslab earthquakes within the Nazca plate in this region are also well studied (e.g., Kausel & Campos, 1992; Peyrat et al., 2006; Ruiz & Madariaga, 2011; Herrera et al., 2017). Additionally, the stress field inferred from interface and intraslab earthquakes is predominantly compressional on the locked plate interface (from 20 km

to about 60 km depth), and mostly extensional within the Nazca plate (Delouis et al., 1996; Bloch et al., 2018).

In contrast, the crustal seismicity in the continental plate in northern Chile has been studied much less. Crustal earthquakes generally have smaller magnitudes, and large-magnitude events are rare. Therefore, earthquake detection and location are challenging, particularly using sparse seismic networks. The 2001 Mw 6.3 Aroma earthquake (Legrand et al., 2007) is the largest instrumentally recorded shallow crustal earthquake in northern Chile, which produced some damage in nearby towns. Despite their generally smaller magnitude, crustal earthquakes pose a significant hazard in northern Chile. For example, it was inferred that seismic activity on crustal offshore faults played a significant role in triggering the 2014 Mw 8.2 Iquique megathrust earthquake (Ruiz et al., 2014; González et al., 2015). In addition, the proximity of active crustal faults to communities causes increased earthquake-related risk.

Two recent earthquake catalogs (Bloch et al., 2014; Sippl et al., 2018) report high-precision detections and locations of interplate, intraslab, and crustal earthquakes in northern Chile. By using dense arrays of permanent and temporary seismic networks, these studies detected and located a considerable number of earthquakes that were previously unreported by the Centro Sismológico Nacional (CSN) of Chile, particularly in the continental crust. These new catalogs show an improved imaging of the seismicity distribution and enable a better analysis of crustal earthquakes and the associated stress field. This provides an opportunity to determine whether fault-slip observations at the surface (e.g., Allmendinger et al., 2005a; Victor et al., 2004) and crustal earthquakes beneath could be created by the same stress field.

In this work, the focal mechanism distribution and stress field in the continental crust of northern Chile are investigated using earthquakes from these two catalogs. High-precision locations and waveforms from dense seismic networks are used to constrain focal mechanisms for smaller events and moment tensors for the largest events. This is allowed by the frequent crustal seismicity detected along the coastal region and in some parts of the Andes (Figure 1). The calculated focal mechanisms are clustered and inverted to infer the spatial variability of the crustal stress field at regional scale.

2 Data set

Origin times and hypocenter locations from Bloch et al. (2014) and Sippl et al. (2018) are used. The Bloch et al. (2014) catalog (catalog 1) contains the 2005-2012 seismicity distribution between 20°S and 21.5°S down to 120 km depth. However, no magnitudes are reported. Abundant crustal seismicity is observed onshore, particularly beneath the Coastal Cordillera and the Andean Precordillera (cross section B-B' in Figure 1). The Sippl et al. (2018) catalog (catalog 2) reports the 2007-2014 seismicity between 18°S and 25°S down to 250 km depth, with a magnitude of completeness of $M_L \sim 2.8$. Most of the crustal seismicity in catalog 2 occurs north of 21.6°S, mostly beneath the Coastal Cordillera, consistent with catalog 1. Although there are surface faults and scarp systems in the Coastal Cordillera (e.g., Allmendinger et al., 2005a), the seismicity underneath this tectonic structure seems to be pervasive, and no evident association to large faults is observed.

Stations from several permanent and temporary seismic networks have operated in northern Chile since 2005. In this work, broadband waveforms were used from the Chilean

National Seismic Network (FDSN code: C), Red Sismológica Nacional (Universidad de Chile, 2013), Global Seismograph Network (ASL/USGS, 1988), IPOC Network (GFZ & CNRS-INSU, 2006), Iquique Local Network (Cesca et al., 2009), Tocopilla Project (Sobiesiak & Schurr, 2007), and Hart-Pisagua Project (Asch et al., 2014), as well as short-period waveforms from the West-Fissure and Atacama-Fault Seismic Network (Wigger et al., 2016).

First, local magnitudes (M_L) were calculated for catalog 1 using the Hutton and Boore (1987) method (Dataset S1), following Sippl et al. (2018). Then, earthquakes within the continental crust were selected from both catalogs considering the 3-D plate interface geometry (Hayes et al., 2018; Sippl et al., 2018) and a maximum depth of 60 km as spatial limits. The crustal subset of catalog 1 shows a magnitude of completeness of $M_L \sim 1.3$, while the subset of slab-related earthquakes shows a higher proportion of large-magnitude events, decreasing the slope of the completeness curve (Supporting Information S1). Finally, the crustal subsets of catalog 1 and catalog 2 (extended to 2017) were combined and repeated events were removed, resulting in a combined catalog from 2005 to 2017.

3 Focal mechanisms and style of faulting

Region-wide, earthquakes with $M_L \geq 3.0$ were selected for focal mechanism calculations. The good coverage of the Wigger et al. (2016) seismic network in the Andean Precordillera around 21°S (cross-section B-B' in Figure 1) aids the study of this region. Because seismicity is less frequent, $M_L \geq 2.0$ earthquakes were selected in the Andes.

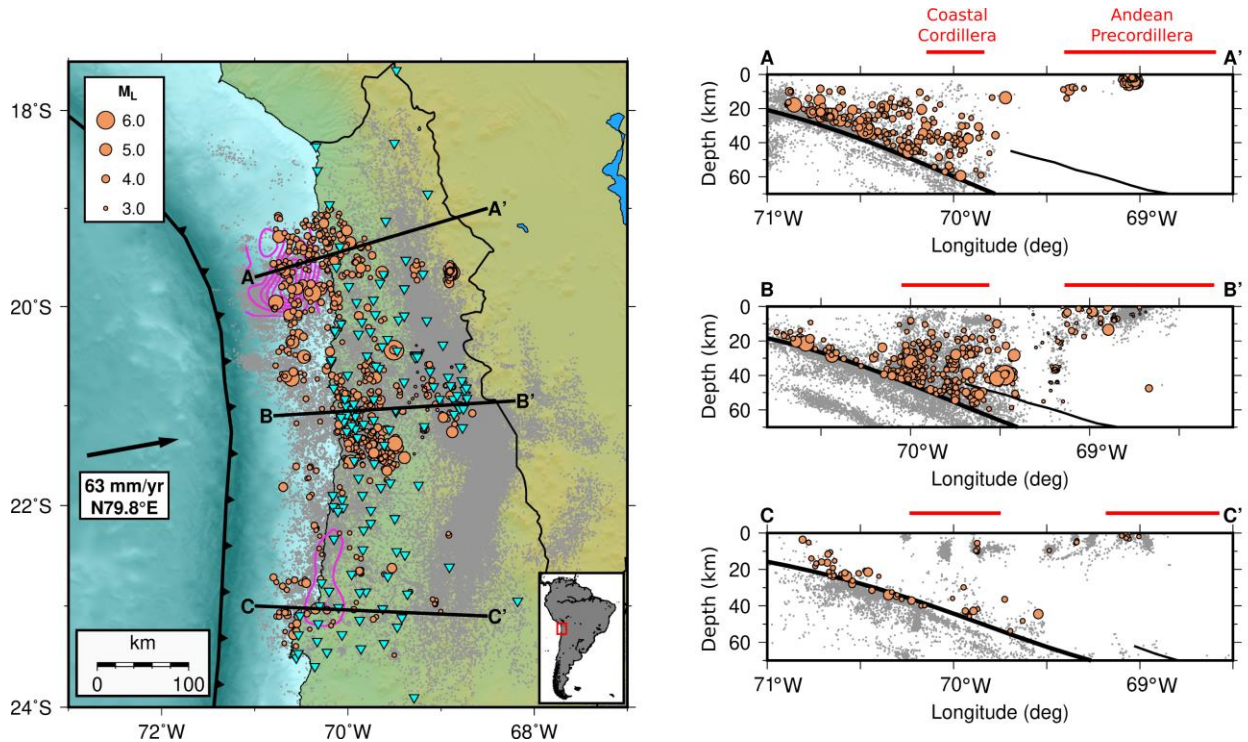


Figure 1: Seismicity in northern Chile reported by Bloch et al. (2014) and Sippl et al. (2018). Coseismic slip of the Tocopilla (Béjar-Pizarro et al., 2010) and Iquique (Ruiz et al., 2014) earthquakes are shown with 1 m purple contours. Stations used in this study are shown with triangles. Large brown circles show the events in the continental lithosphere with at least five

unambiguous P-wave polarities. The rest of the seismicity is shown with grey dots. Convergence vector from Kendrick et al. (2003) and trench location from Bird (2003). The inset shows the location of the map within South America. Cross sections show the plate interface (Hayes et al., 2018) and the continental Moho (Yuan et al., 2000) with tick and thin lines, respectively.

For the selected events, seismograms recorded within 300 km epicentral distance were integrated and a 1 Hz high-pass filter was applied. P-wave polarities were picked from the vertical components and S/P amplitude ratios were calculated from the maximum S- and P-wave amplitudes of the three-component Cartesian sum. Azimuth and takeoff angles were calculated using ray propagation through the Husen et al. (1999) 1-D velocity model. Finally, polarities and amplitude ratios were inverted with HASH (Hardebeck & Shearer, 2002, 2003) to obtain the optimal double-couple focal mechanism that fits the observed radiation pattern. The stability of the solution was considered by randomly perturbing the azimuth and takeoff angles by 5° in the inversion. Based on the solution stability (spread of the set of solutions with respect to the preferred solution), the focal mechanism quality was assigned to one of four classes ranging from A (stable solution) to D (unstable solution) (Supporting Information S2). This analysis resulted in a focal mechanism catalog of 817 crustal events that have at least 5 unambiguous polarity observations (Dataset S2).

Full moment tensor (MT) inversions were carried out for the largest earthquakes ($M_L \geq 4.5$). Regional Green's functions were precalculated for the Husen et al. (1999) layered earth model using the Fomosto QSEIS code (Wang, 1999). The broadband velocity seismograms were inverted using the BEAT software (Vasyura-Bathke et al., 2020), which uses a nonlinear approach to estimate the full MT. Waveforms were modeled in various frequency bands defined within the 0.02 and 0.15 Hz range. The sequential Monte Carlo method (Del Moral et al., 2006) was used to sample the parameter space (centroid location, source time function, and components of the full MT). With this method, proper waveform modeling was achieved for seven $M_L \geq 4.5$ crustal earthquakes. The resulting MT components, uncertainties and waveforms are shown in Supporting Information S3. Overall, the full MT results confirm the fault geometries and pressure (P) and tension (T) axis orientations obtained with HASH, with relatively low ($\sim 20^\circ$) Kagan angles (Kagan, 1991) between the two methods for five of the seven events (Supporting Information S4). The differences on fault orientations between HASH and BEAT could be attributable to station coverage limitations affecting the HASH solution, limitations of the velocity model, or a complex rupture propagation that is better represented by an MT solution. This could be the case for the largest event, which exhibits the largest Kagan angle between the two methods.

Figure 2 summarizes the predominant faulting types and P-axis orientations of the best focal mechanism solutions. This is a subset of 355 events that only considers quality A and B mechanisms that had at least 10 unambiguous polarity observations and a stereographic station gap smaller than 180° . P-axes of offshore and onshore events along the coast show a predominantly margin-parallel orientation, especially beneath the Coastal Cordillera (Figure 2a). This is consistent with the mechanisms of coastal events reported by González et al. (2015). Ternary plots (Kaverina et al., 1996; Álvarez-Gómez, 2014) in Figure 2b show that these mechanisms in the coastal region correspond to predominantly reverse (thrust) earthquakes, which occur throughout the crust. Their orientations appear to be stationary in time over the decade of observations, particularly for the onshore events, which are not affected by the

occurrence of large interplate earthquakes (Figure 2c). Conversely, P-axis orientations of the seismicity in the Andean Precordillera (east of 69.4°W at 21°S) show a predominantly NE-SW orientation (Figure 2a). The faulting style corresponds to mostly shallow strike-slip mechanisms (some of them with oblique component), and some deeper normal-faulting events (Figure 2b). These results suggest a different faulting style in the Andean Precordillera compared with the coastal region.

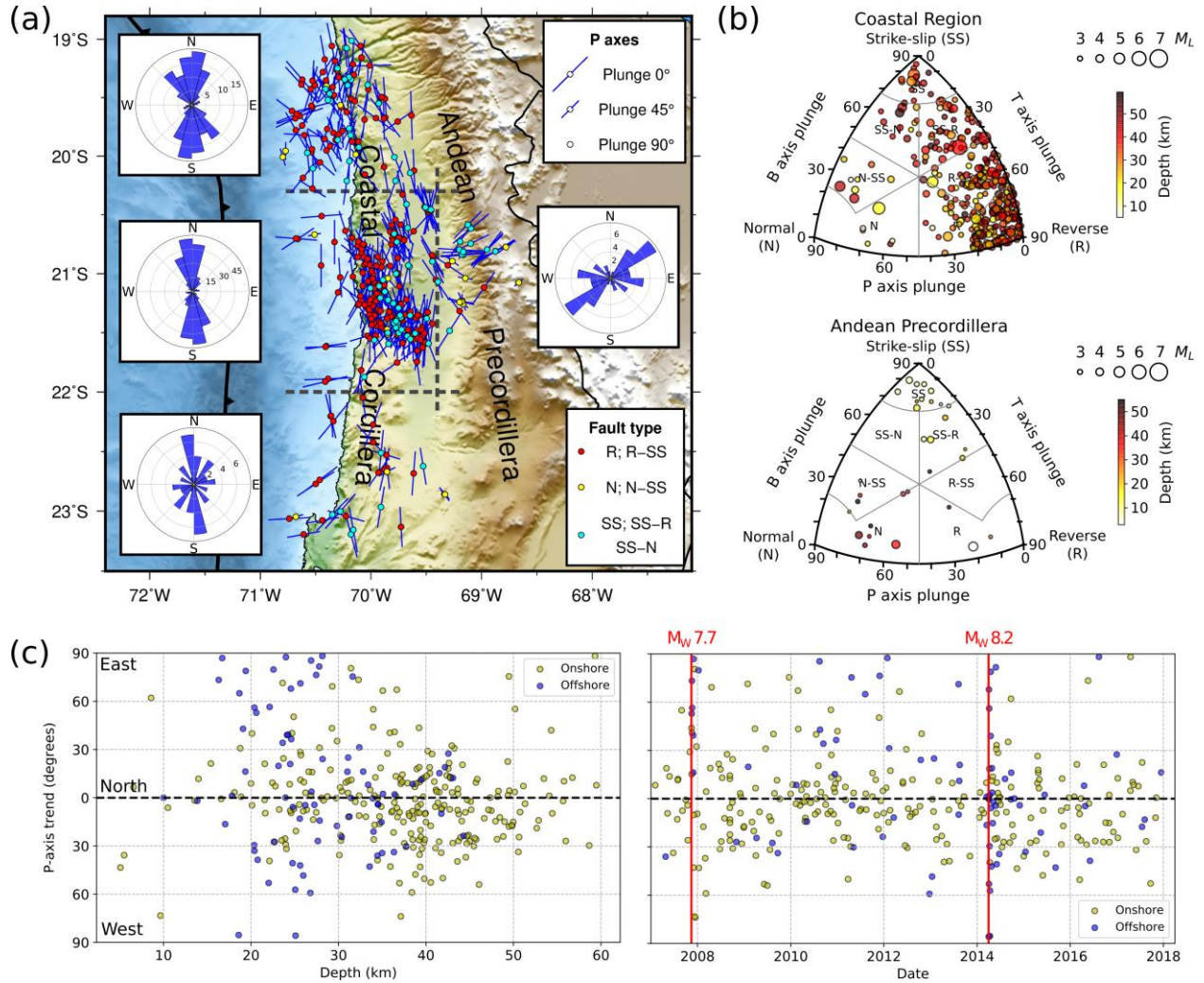


Figure 2: Fault characterization of crustal earthquakes. (a) Spatial distribution of fault types and P-axis orientations obtained from focal mechanisms. Rose diagrams summarize dominant P-axis trends on areas delimited by grey dashed lines. (b) Ternary plots characterizing the type of faulting in the Coastal and Andes regions. (c) P-axis trend distribution as a function of depth and time for events that occurred in the coastal region. The 2007 Tocopilla and 2014 Iquique earthquakes are highlighted with red lines.

4 Stress field

The Bayesian method developed by Arnold and Townend (2007) was used to estimate the stress tensor by inverting the strike, dip, and rake angles of a group of focal mechanisms,

considering focal mechanism uncertainties. The subset of best focal mechanisms (355 events in Figure 2) was used as input data to estimate the crustal stress field in northern Chile. The RMS angle obtained from HASH (Supporting Information S2) was used to define the average uncertainty of each focal mechanism. The method estimates the three stress tensor components ($S_1 > S_2 > S_3$), the stress ratio $R = (S_2 - S_3)/(S_1 - S_3)$ that describes the shape of the stress ellipsoid, and the maximum horizontal compressive stress direction, S_{Hmax} (Lund & Townend, 2007).

To analyze the spatial variability of the stress field, seismicity was divided into groups and a stress tensor was calculated for each group. Following Balfour et al. (2011), we assumed that the stress is constant throughout the crust thickness. Seismicity along the Coastal Cordillera was divided into groups at equal latitudinal spacing, and the seismicity in the Andean Precordillera around 21°S was defined as another group.

Stress field results are summarized in Figure 3 and Supporting Information S5. Stress tensors reflect the clear trends shown by the focal mechanisms. The stress tensors A, B, C, and D along the coast show well-constrained components, where S_1 and S_3 are almost horizontal and vertical, respectively, due to the predominance of thrust earthquakes in the region. S_{Hmax} of the four stress tensors along the coastal region show a clear horizontal margin-parallel compression. Stress tensor E, located in the Andean Precordillera, exhibits larger uncertainties for its components due to the smaller number of events and the more balanced occurrence of strike-slip and normal events. This stress tensor shows a predominantly strike-slip regime in this area, with nearly horizontal S_1 and S_3 components, and an S_{Hmax} oriented ENE-WSW. The orientation of tensor E is consistent with the stress tensor obtained by Salazar et al. (2017) for this area.

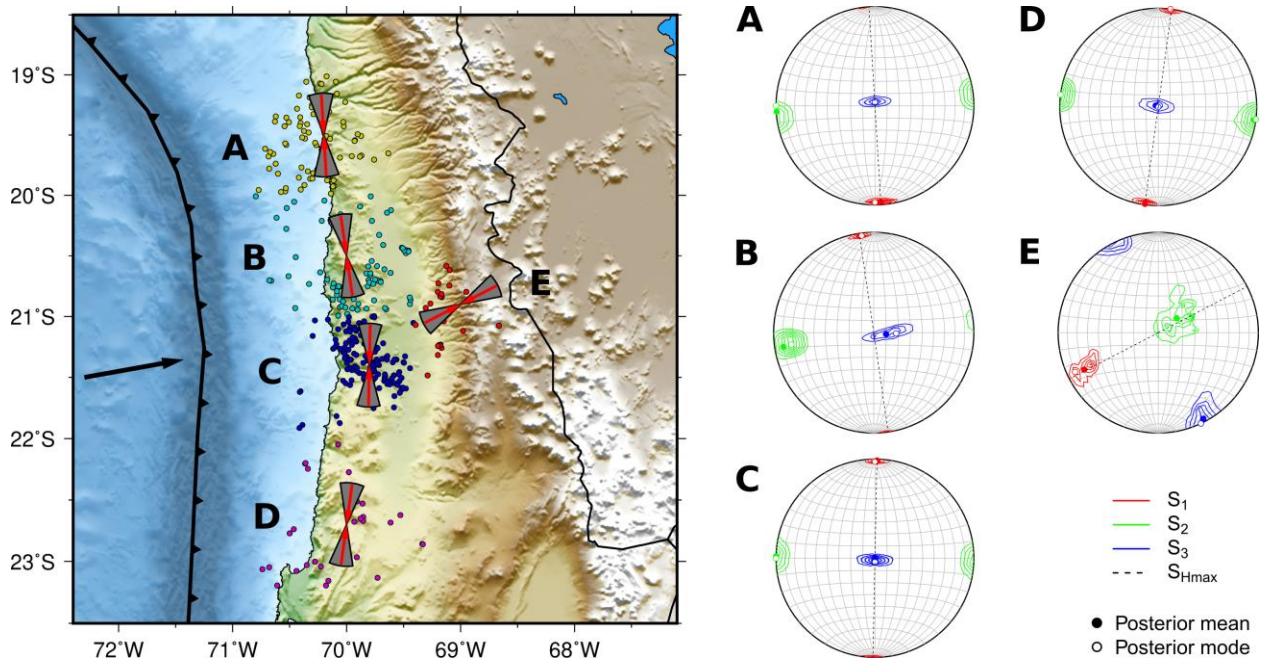


Figure 3: Crustal stress field in northern Chile. Red arrows on the map show the direction of S_{Hmax} with wedges that show the 95% credibility interval of the result. Stereographic projections of the stress tensors are shown on the right. Contours show the posterior probability densities of the three principal stress components.

5 Discussion

Pervasive seismicity occurs throughout the crust in the coastal region. These earthquakes have mostly reverse mechanisms with margin-parallel P-axes at all depths, indicating a margin-parallel compressional stress field in the region. These results are even clearer for the onshore events beneath the Coastal Cordillera (Figure 2c). This likely indicates an abrupt change of stress regime from the plate interface to the overlying crust in the coastal region.

The Coastal Cordillera in northern Chile is the remnant of a magmatic arc that was active during the Jurassic and early Cretaceous periods of the Mesozoic era (e.g., Mpodozis & Ramos, 1990), during the birth of the modern Andes. Its most important structure is the Mesozoic-Cenozoic Atacama Fault System (AFS) (e.g., González et al., 2003; Cembrano et al., 2007), extending from 21°S to 29.5°S with mostly normal and dextral strike-slip faults. Additionally, the Coastal Cordillera features several scarps between 19°S and 21.6°S striking perpendicular to the margin with reverse-fault kinematics, indicating a margin-parallel shortening (Allmendinger et al., 2005a). Geochronology analysis suggests that these scarps are more recent, having been active during the late Miocene and Pliocene periods (Allmendinger et al., 2005a), with some still active today (Allmendinger & González, 2010). These scarps and the crustal earthquakes occurring beneath exhibit the same fault kinematics and compression direction (Figures 2a and 4a), indicating that both may have been created by the current crustal stress field, which could then be long-lasting.

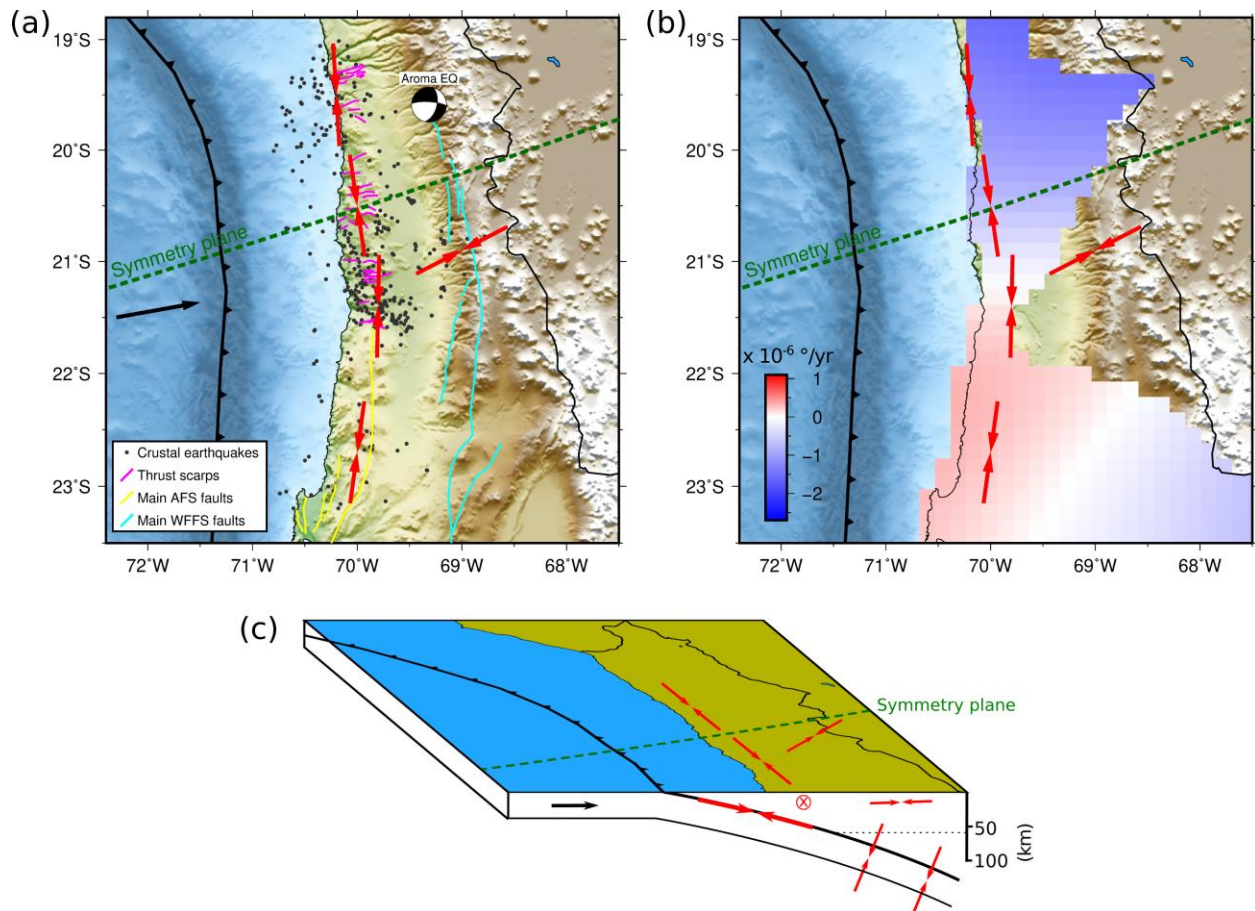


Figure 4: Interpretation of the crustal stress field. (a) S_{Hmax} orientations (red arrows) in a seismotectonic context. The focal mechanism shows the 2001 Mw 6.3 Aroma earthquake (Legrand et al., 2007). (b) S_{Hmax} orientations within the vertical axis rotation rate data (R.W. Allmendinger pers. comm.). (c) Red arrows and the cross in the cartoon correspond to the S_1 orientations obtained in this study for the crust and by Bloch et al. (2018) for the slab-related stress.

Margin-parallel compression in the continental crust has also been observed in other concave subduction regions; for example, in Cascadia (e.g., Johnson et al., 2004; Balfour et al., 2011) and in Japan (e.g., Kusunoki & Kimura, 1998). For northern Chile, it could be a consequence of deformation partition from the main subduction direction controlled by two mechanisms acting together: (1) The concave margin geometry shaping the Bolivian Orocline, coupled with an oblique plate convergence motion. The symmetry plane of the entire Andean orogen (Gephart, 1994) crosses northern Chile roughly in the center of our study area (Figure 4), indicating maximum concavity in this region and a change in sign of vertical axis rotation rates observed by GNSS and paleomagnetic data (Allmendinger et al., 2005b, 2007) (Figure 4b). This geometry evokes along-strike bending of the orocline's inner arc (coastal region), creating margin-parallel shortening in the area. (2) From 3-D thermomechanical experiments, Boutelier et al. (2014) found that high friction on the plate interface is required to generate margin-parallel shortening in a concave subduction zone. In this context, northern Chile exhibits large patches of intermediate and nearly full interseismic coupling on the plate interface (Métois et al., 2016), which could enhance the deformation of the orocline. These two factors may be responsible for the margin-parallel compressive crustal stress field inferred in this study, for the thrust scarps observed in the Coastal Cordillera (Allmendinger et al., 2005a), and for the change of vertical axis rotation rates from counterclockwise north of the symmetry plane to clockwise south of it, as summarized in Figures 4a and 4b.

The stress field beneath the Andean Precordillera was analyzed only in a local region around 21°S (east of 69.4°W in cross-section B-B' in Figure 1), where good station coverage allowed the calculation of high-quality focal mechanisms in the Andes. Seismicity in this area shows a west-dipping distribution following a rheological boundary (350°C isotherm), where fluid migration may facilitate seismicity occurrence (Bloch et al., 2014; Salazar et al., 2017). Stress tensor E in Figure 3 shows that this area exhibits a strike-slip regime with an ENE-WSW oriented S_{Hmax} that is nearly parallel to the plate convergence direction. The observed shallow strike-slip earthquakes seem to make the largest contribution to the stress tensor. Our set of best focal mechanisms for this area is smaller and less diverse than that reported by Salazar et al. (2017); nevertheless, the resulting stress tensor from the two studies is highly consistent.

The main structure in this area of the Andean Precordillera is the West Fissure Fault System (WFFS), featuring faults with diverse slip kinematics striking sub-parallel to the margin (e.g., Victor et al., 2004; Salazar et al., 2017). In particular, a strike-slip fault regime has been observed in higher altitude areas of the Andean Precordillera (Victor et al., 2004; Farías et al., 2005), near the locations of the shallow strike-slip earthquakes shown in Figure 2. The local vertical stresses exerted by the gravitational forces of the elevated topography have been proposed to be the cause of the strike-slip regime in the Andes (Salazar et al., 2017). These forces change the regime from reverse faulting at lower altitudes to strike-slip faulting at higher altitudes, since the increase of the vertical stress at higher altitudes would surpass the minimum

horizontal stress component, resulting in a nearly vertical S_2 component. Similar spatial variations of stress orientations with topography have also been observed in the arc-backarc region of Japan (Yoshida et al., 2015).

Although it was not possible to analyze more earthquakes over a wider area in the Andean Precordillera, there is evidence of a dextral strike-slip regime in the Andes between 19°S and 21°S (Farías et al., 2005). In fact, the large 2001 M_w 6.3 Aroma crustal earthquake ruptured on a dextral strike-slip fault (Legrand et al., 2007) in the Andean Precordillera near 19.5°S (Figure 4a). Its kinematics are consistent with our stress regime inferred further south.

6 Conclusions

A focal mechanism catalog of crustal earthquakes and the associated crustal stress field were inferred for northern Chile. The catalog contains focal mechanisms of 817 earthquakes. A subset of 355 earthquakes with high-quality focal mechanisms were inverted for the crustal stress field.

To date, this data set provides the most complete estimate and coverage of the contemporary crustal stress field in northern Chile. Crustal stress field results show different regimes for the Coastal Cordillera and the Andean Precordillera. The Coastal Cordillera region exhibits margin-parallel compression within a reverse-fault regime, which is consistent with the fault kinematics of the scarps observed in the region. This could be due to the interplay of a concave margin geometry and a coupled plate interface that extends down to 60 km depth (Figure 4c), creating a bending of this coastal region (inner arc of the Bolivian Orocline). Conversely, the strike-slip regime observed in the Andean Precordillera suggests a different deformation regime. Its S_{Hmax} direction is oriented nearly parallel to the plate convergence direction. This regime could mostly result from local stresses imposed by the thicker crust in the higher Andes. In the future, the deployment of dense seismic networks over a wider area into the Andean Orogen will allow a better determination of the spatial extent of the inferred crustal stress field.

Acknowledgments and Data

This research was supported by Natural Sciences and Engineering Research Council of Canada (NSERC) grants and funding from the University of Victoria. Waveform data were downloaded from the Federation of Digital Seismograph Networks (FDSN) web services using the ObsPy toolkit (Beyreuther et al., 2010). ObsPy was also used to process the downloaded seismic data. Maps were created using Generic Mapping Tools (Wessel et al., 2013).

References

Allmendinger, R. W., González, G., Yu, J., Hoke, G., & Isacks, B. (2005a). Trench-parallel shortening in the Northern Chilean Forearc: Tectonic and climatic implications. *Geological Society of America Bulletin*, 117(1-2), 89-104. <https://doi.org/10.1130/B25505.1>

- 328 Allmendinger, R. W., Smalley Jr, R., Bevis, M., Caprio, H., & Brooks, B. (2005b). Bending the
329 Bolivian orocline in real time. *Geology*, 33(11), 905-908. <https://doi.org/10.1130/G21779.1>
- 330 Allmendinger, R. W., Reilinger, R., & Loveless, J. (2007). Strain and rotation rate from GPS in
331 Tibet, Anatolia, and the Altiplano. *Tectonics*, 26(3). <https://doi.org/10.1029/2006TC002030>
- 332 Allmendinger, R. W., & González, G. (2010). Invited review paper: Neogene to Quaternary
333 tectonics of the coastal Cordillera, northern Chile. *Tectonophysics*, 495(1-2), 93-110.
334 <https://doi.org/10.1016/j.tecto.2009.04.019>
- 335 Álvarez-Gómez, J. A. (2014). *FMC: a one-liner Python program to manage, classify and plot*
336 *focal mechanisms*. Paper presented at EGU General Assembly, Vienna, Austria.
- 337 Arnold, R., & Townend, J. (2007). A Bayesian approach to estimating tectonic stress from
338 seismological data. *Geophysical Journal International*, 170(3), 1336-1356.
339 <https://doi.org/10.1111/j.1365-246X.2007.03485.x>
- 340 Asch, G., Tilmann, F., Heit, B., & Schurr, B. (2014). HART-PISAGUA Project Chile. *GFZ Data*
341 *Services*. Other/Seismic Network. <http://doi.org/10.14470/8Q7569558037>
- 342 ASL/USGS (1988). Global Seismograph Network (GSN - IRIS/USGS). *International*
343 *Federation of Digital Seismograph Networks*. <https://doi.org/10.7914/SN/IU>
- 344 Balfour, N. J., Cassidy, J. F., Dosso, S. E., & Mazzotti, S. (2011). Mapping crustal stress and
345 strain in southwest British Columbia. *Journal of Geophysical Research: Solid Earth*, 116(B3).
346 <https://doi.org/10.1029/2010JB008003>
- 347 Béjar-Pizarro, M., Carrizo, D., Socquet, A., Armijo, R., Barrientos, S., Bondoux, F., et al.
348 (2010). Asperities and barriers on the seismogenic zone in North Chile: state-of-the-art after the
349 2007 M w 7.7 Tocopilla earthquake inferred by GPS and InSAR data. *Geophysical Journal*
350 *International*, 183(1), 390-406. <https://doi.org/10.1111/j.1365-246X.2010.04748.x>
- 351 Beyreuther, M., Barsch, R., Krischer, L., Megies, T., Behr, Y., & Wassermann, J. (2010). ObsPy:
352 A Python toolbox for seismology. *Seismological Research Letters*, 81(3), 530-533.
353 <https://doi.org/10.1785/gssrl.81.3.530>
- 354 Bird, P. (2003). An updated digital model of plate boundaries. *Geochemistry, Geophysics,*
355 *Geosystems*, 4(3). <https://doi.org/10.1029/2001GC000252>
- 356 Bloch, W., Kummerow, J., Salazar, P., Wigger, P., & Shapiro, S. A. (2014). High-resolution
357 image of the North Chilean subduction zone: seismicity, reflectivity and fluids. *Geophysical*
358 *Journal International*, 197(3), 1744-1749. <https://doi.org/10.1093/gji/ggu084>
- 359 Bloch, W., Schurr, B., Kummerow, J., Salazar, P., & Shapiro, S. A. (2018). From slab coupling
360 to slab pull: Stress segmentation in the subducting Nazca plate. *Geophysical Research Letters*,
361 45(11), 5407-5416. <https://doi.org/10.1029/2018GL078793>
- 362 Boutelier, D., Oncken, O., & Cruden, A. R. (2014). Trench-parallel shortening in the forearc
363 caused by subduction along a seaward-concave plate boundary: Insights from analogue
364 modelling experiments. *Tectonophysics*, 611, 192-203.
365 <https://doi.org/10.1016/j.tecto.2013.11.028>

- Cembrano, J., Lavenu, A., Yañez, G., Riquelme, R., García, M., González, G., & Hérail, G. (2007). Neotectonics. In T. Moreno & W. Gibbons (Eds.), *The Geology of Chile* (pp. 231-261). London, UK: Geological Society of London. <https://doi.org/10.1144/GOCH>
- Cesca, S., Sobiesiak, M., Tassara, A., Olcay, M., Günther, E., Mikulla, S., & Dahm, T. (2009). The Iquique Local Network and PicArray. *GFZ Data Services*. Other/Seismic Network. <https://doi.org/10.14470/VD070092>
- Del Moral, P., Doucet, A., & Jasra, A. (2006). Sequential monte carlo samplers. *Journal of the Royal Statistical Society: Series B (Statistical Methodology)*, 68(3), 411-436. <https://doi.org/10.1111/j.1467-9868.2006.00553.x>
- Delouis, B., Cisternas, A., Dorbath, L., Rivera, L., & Kausel, E. (1996). The Andean subduction zone between 22 and 25°S (northern Chile): Precise geometry and state of stress. *Tectonophysics*, 259(1-3), 81-100. [https://doi.org/10.1016/0040-1951\(95\)00065-8](https://doi.org/10.1016/0040-1951(95)00065-8)
- Farías, M., Charrier, R., Comte, D., Martinod, J., & Hérail, G. (2005). Late Cenozoic deformation and uplift of the western flank of the Altiplano: Evidence from the depositional, tectonic, and geomorphologic evolution and shallow seismic activity (northern Chile at 19°30' S). *Tectonics*, 24(4). <https://doi.org/10.1029/2004TC001667>
- Gephart, J. W. (1994). Topography and subduction geometry in the central Andes: Clues to the mechanics of a noncollisional orogen. *Journal of Geophysical Research: Solid Earth*, 99(B6), 12279-12288. <https://doi.org/10.1029/94JB00129>
- González, G., Cembrano, J., Carrizo, D., Macci, A., & Schneider, H. (2003). The link between forearc tectonics and Pliocene–Quaternary deformation of the Coastal Cordillera, northern Chile. *Journal of South American Earth Sciences*, 16(5), 321-342. [https://doi.org/10.1016/S0895-9811\(03\)00100-7](https://doi.org/10.1016/S0895-9811(03)00100-7)
- González, G., Salazar, P., Loveless, J. P., Allmendinger, R. W., Aron, F., & Shrivastava, M. (2015). Upper plate reverse fault reactivation and the unclamping of the megathrust during the 2014 northern Chile earthquake sequence. *Geology*, 43(8), 671-674. <https://doi.org/10.1130/G36703.1>
- GFZ & CNRS-INSU. (2006). IPOC Seismic Network. Integrated Plate boundary Observatory Chile – IPOC. Other/Seismic Network. <https://doi.org/10.14470/PK615318>
- Hardebeck, J. L., & Shearer, P. M. (2002). A new method for determining first-motion focal mechanisms. *Bulletin of the Seismological Society of America*, 92(6), 2264-2276. <https://doi.org/10.1785/0120010200>
- Hardebeck, J. L., & Shearer, P. M. (2003). Using S/P amplitude ratios to constrain the focal mechanisms of small earthquakes. *Bulletin of the Seismological Society of America*, 93(6), 2434-2444. <https://doi.org/10.1785/0120020236>
- Hayes, G. P., Moore, G. L., Portner, D. E., Hearne, M., Flamme, H., Furtney, M., & Smoczyk, G. M. (2018). Slab2, a comprehensive subduction zone geometry model. *Science*, 362(6410), 58-61. <https://doi.org/10.1126/science.aat4723>
- Herrera, C., Ruiz, S., Madariaga, R., & Poli, P. (2017). Dynamic inversion of the 2015 Jujuy earthquake and similarity with other intraslab events. *Geophysical Journal International*, 209(2), 866-875. <https://doi.org/10.1093/gji/ggx056>

- Husen, S., Kissling, E., Flueh, E., & Asch, G. (1999). Accurate hypocentre determination in the seismogenic zone of the subducting Nazca Plate in northern Chile using a combined on-/offshore network. *Geophysical Journal International*, 138(3), 687-701. <https://doi.org/10.1046/j.1365-246x.1999.00893.x>
- Hutton, L. K., & Boore, D. M. (1987). The M_L scale in southern California. *Bulletin of the Seismological Society of America*, 77(6), 2074-2094.
- Johnson, S. Y., Blakely, R. J., Stephenson, W. J., Dadisman, S. V., & Fisher, M. A. (2004). Active shortening of the Cascadia forearc and implications for seismic hazards of the Puget Lowland. *Tectonics*, 23(1). <https://doi.org/10.1029/2003TC001507>
- Kagan, Y. Y. (1991). 3-D rotation of double-couple earthquake sources. *Geophysical Journal International*, 106(3), 709-716. <https://doi.org/10.1111/j.1365-246X.1991.tb06343.x>
- Kausel, E., & Campos, J. (1992). The $M_s=8$ tensional earthquake of 9 December 1950 of northern Chile and its relation to the seismic potential of the region. *Physics of the earth and planetary interiors*, 72(3-4), 220-235. [https://doi.org/10.1016/0031-9201\(92\)90203-8](https://doi.org/10.1016/0031-9201(92)90203-8)
- Kaverina, A. N., Lander, A. V., & Prozorov, A. G. (1996). Global creepex distribution and its relation to earthquake-source geometry and tectonic origin. *Geophysical Journal International*, 125(1), 249-265. <https://doi.org/10.1111/j.1365-246X.1996.tb06549.x>
- Kendrick, E., Bevis, M., Smalley Jr, R., Brooks, B., Vargas, R. B., Lauria, E., & Fortes, L. P. S. (2003). The Nazca–South America Euler vector and its rate of change. *Journal of South American Earth Sciences*, 16(2), 125-131. [https://doi.org/10.1016/S0895-9811\(03\)00028-2](https://doi.org/10.1016/S0895-9811(03)00028-2)
- Kusunoki, K., & Kimura, G. (1998). Collision and extrusion at the Kuril-Japan arc junction. *Tectonics*, 17(6), 843-858. <https://doi.org/10.1029/98TC02699>
- Legrand, D., Delouis, B., Dorbath, L., David, C., Campos, J., Marquez, L., et al. (2007). Source parameters of the $M_w=6.3$ Aroma crustal earthquake of July 24, 2001 (northern Chile), and its aftershock sequence. *Journal of south American earth sciences*, 24(1), 58-68. <https://doi.org/10.1016/j.jsames.2007.02.004>
- Lund, B., & Townend, J. (2007). Calculating horizontal stress orientations with full or partial knowledge of the tectonic stress tensor. *Geophysical Journal International*, 170(3), 1328-1335. <https://doi.org/10.1111/j.1365-246X.2007.03468.x>
- Métois, M., Vigny, C., & Socquet, A. (2016). Interseismic coupling, megathrust earthquakes and seismic swarms along the Chilean subduction zone (38–18 S). *Pure and Applied Geophysics*, 173(5), 1431-1449. <https://doi.org/10.1007/s00024-016-1280-5>
- Mpodozis, C., & Ramos, V. (1990). The Andes of Chile and Argentina. In G.E. Ericksen, M.T. Cañas Pinochet, J.A. Reinemund (Eds.), *Geology of the Andes and its relation to hydrocarbon and mineral resources*, Earth Science Series (Vol. 11, pp. 59-90). Houston, Texas: Circum-Pacific Council for Energy and Mineral Resources.
- Peyrat, S., Campos, J., De Chabalier, J. B., Perez, A., Bonvalot, S., Bouin, M. P., et al. (2006). Tarapacá intermediate depth earthquake (M_w 7.7, 2005, northern Chile): A slab pull event with horizontal fault plane constrained from seismologic and geodetic observations. *Geophysical Research Letters*, 33(22). <https://doi.org/10.1029/2006GL027710>

- Peyrat, S., Madariaga, R., Bufo, E., Campos, J., Asch, G., & Vilotte, J. P. (2010). Kinematic rupture process of the 2007 Tocopilla earthquake and its main aftershocks from teleseismic and strong-motion data. *Geophysical Journal International*, 182(3), 1411-1430. <https://doi.org/10.1111/j.1365-246X.2010.04685.x>
- Ruegg, J. C., Campos, J., Armijo, R., Barrientos, S., Briole, P., Thiele, R., et al. (1996). The Mw=8.1 Antofagasta (North Chile) earthquake of July 30, 1995: First results from teleseismic and geodetic data. *Geophysical Research Letters*, 23(9), 917-920. <https://doi.org/10.1029/96GL01026>
- Ruiz, S., Metois, M., Fuenzalida, A., Ruiz, J., Leyton, F., Grandin, R., et al. (2014). Intense foreshocks and a slow slip event preceded the 2014 Iquique Mw 8.1 earthquake. *Science*, 345(6201), 1165-1169. <https://doi.org/10.1126/science.1256074>
- Ruiz, S., & Madariaga, R. (2011). Determination of the friction law parameters of the Mw 6.7 Michilla earthquake in northern Chile by dynamic inversion. *Geophysical Research Letters*, 38(9). <https://doi.org/10.1029/2011GL047147>
- Ruiz, S., & Madariaga, R. (2018). Historical and recent large megathrust earthquakes in Chile. *Tectonophysics*, 733, 37-56. <https://doi.org/10.1016/j.tecto.2018.01.015>
- Salazar, P., Kummerow, J., Wigger, P., Shapiro, S., & Asch, G. (2017). State of stress and crustal fluid migration related to west-dipping structures in the slab-forearc system in the northern Chilean subduction zone. *Geophysical Journal International*, 208(3), 1403-1413. <https://doi.org/10.1093/gji/ggw463>
- Sippl, C., Schurr, B., Asch, G., & Kummerow, J. (2018). Seismicity structure of the northern Chile forearc from > 100,000 double-difference relocated hypocenters. *Journal of Geophysical Research: Solid Earth*, 123(5), 4063-4087. <https://doi.org/10.1002/2017JB015384>
- Sobiesiak, M., & Schurr, B. (2007). Tocopilla Project. *GFZ Data Services*. Other/Seismic Network. <http://doi.org/10.14470/L47552843299>
- Soto, H., Sippl, C., Schurr, B., Kummerow, J., Asch, G., Tilmann, F., et al. (2019). Probing the Northern Chile Megathrust with Seismicity: The 2014 M 8.1 Iquique Earthquake Sequence. *Journal of Geophysical Research: Solid Earth*, 124(12), 12935-12954. <https://doi.org/10.1029/2019JB017794>
- Universidad de Chile (2013). Red Sismológica Nacional. *International Federation of Digital Seismograph Networks*. <https://doi.org/10.7914/SN/C1>
- Vasyura-Bathke, H., Dettmer, J., Steinberg, A., Heimann, S., Isken, M. P., Zielke, O., et al. (2020). The Bayesian Earthquake Analysis Tool. *Seismological Research Letters*, 91(2A), 1003-1018. <https://doi.org/10.1785/0220190075>
- Victor, P., Oncken, O., & Glodny, J. (2004). Uplift of the western Altiplano plateau: Evidence from the Precordillera between 20° and 21°S (northern Chile). *Tectonics*, 23(4). <https://doi.org/10.1029/2003TC001519>
- Wang, R. (1999). A simple orthonormalization method for stable and efficient computation of Green's functions. *Bulletin of the Seismological Society of America*, 89(3), 733-741.

- 486 Wessel, P., Smith, W. H., Scharroo, R., Luis, J., & Wobbe, F. (2013). Generic mapping tools:
487 improved version released. *Eos, Transactions American Geophysical Union*, 94(45), 409-410.
488 <https://doi.org/10.1002/2013EO450001>
- 489 Wigger, P., Salazar, P., Kummerow, J., Bloch, W., Asch, G., & Shapiro, S. (2016). West--
490 Fissure- and Atacama-Fault Seismic Network (2005/2012). *Deutsches GeoForschungsZentrum*
491 *GFZ*. Other/Seismic Network. <http://doi.org/10.14470/3S7550699980>
- 492 Yoshida, K., Hasegawa, A., & Okada, T. (2015). Spatial variation of stress orientations in NE
493 Japan revealed by dense seismic observations. *Tectonophysics*, 647, 63-72.
494 <https://doi.org/10.1016/j.tecto.2015.02.013>
- 495 Yuan, X., Sobolev, S. V., Kind, R., Oncken, O., Bock, G., Asch, G., et al. (2000). Subduction
496 and collision processes in the Central Andes constrained by converted seismic
497 phases. *Nature*, 408(6815), 958-961. <https://doi.org/10.1038/35050073>